Preparation of multifunctional nanocomposites Fe_3O_4@SiO_2–EDTA and its adsorption of heavy metal ions in water solution

Tao Gong and Yongbai Tang

ABSTRACT

Novel magnetic Fe_3O_4@SiO_2-ethylenediamine tetraacetic acid (adsorbent) CMS–COOH-modified magnetic materials, CMS was prepared by surface modification of amino-functionalized Fe_3O_4@SiO_2 (–NH_2-modified magnetic materials, NMS) with EDTA using water-soluble carbodiimide as the cross-linker in deionized water solution. The phase structure, infrared spectra, thermal analysis and magnetic properties of were characterized by X-ray diffraction, Fourier-transform infrared spectroscopy, thermogravimetric analysis, and vibrating sample magnetometry and its properties for removal of heavy metal ions under varied experimental conditions were also investigated. The results revealed that CMS had good tolerance to low pH and exhibited good removal efficiency for the metal ions. The maximum adsorption capacities of CMS were found to be 0.11 mmol g^{-1} for Cu(II) at pH5.0 (30 °C) and 0.14 mmol g^{-1} for Pb(II) ions at pH2.0 (30 °C).

Key words | adsorption, EDTA, Fe_3O_4 nanoparticles, heavy metal, magnetic separation, modification

Tao Gong
Yongbai Tang (corresponding author)
College of Materials Science and Engineering,
Sichuan University,
Chengdu 610000,
China
E-mail: *tangyongbai@163.com*

INTRODUCTION

With the rapid development of electroplating equipment, mining, tanneries, batteries, paper, fertilizers, and pesticides, more and more heavy metal wastewater is directly or indirectly discharged into the environment, which has a serious impact on the ecosystem. Unlike organic pollutants, heavy metals are not biodegradable and accumulate in living organisms (Awual *et al.* 2014; Dong *et al.* 2015); therefore, heavy metal pollution is a major problem in today's society. There are many methods for removing heavy metal ions, such as ion exchange method (Gode & Pehlivan 2006), chemical precipitation method (Fu & Wang 2011), electrochemical treatment (Nanseu-Njiki *et al.* 2009), membrane separation method (Landaburu-Aguirre *et al.* 2010), biochemical method (Wu *et al.* 2010), adsorption method (Baccar *et al.* 2009; Ali 2012; Sharififard *et al.* 2012; Ren *et al.* 2013; Sun *et al.* 2013; Kong *et al.* 2014; Cegłowski & Schroeder 2015) and so on. In these methods, the adsorption method is suitable for low ion concentration wastewater and large adsorption amount, but the selection of adsorbents is particularly important. The adsorbents currently used include carbon-based materials, mineral materials, metal oxide materials, ion-selective materials, and biological materials. Magnetic nanoparticles (MNPs, such as ferroferic oxide, Fe_3O_4) have also been extensively studied due to their superparamagnetism, which make them easy to separate from water (Zargoosh *et al.* 2014; Zhang *et al.* 2014). In addition, magnetic materials possess a larger surface area and can be synthesized by simpler methods (Cheng *et al.* 2012). However, the agglomeration of Fe_3O_4 in water reduces the active sorption sites and weakens its adsorption capacity (Zhang *et al.* 2014). Many experiments have shown that proper surface functionalization can solve this problem and enhance the stability and performance of Fe_3O_4 MNPs (Kim *et al.* 2013).

MNPs have undergone many modifications, including thiol functionalization and amino functionalization, and MNPs modified with poly(2-aminoethyl methacrylate hydrochloride), dithiocarbamate, (3-aminopropyl) triethoxysilane, and polydopamine have a distinct affinity to combine with Cu(II), Hg(II), Ag(II), Cd(II), Pb(II), Co(II), Ni(II), and Cr(III) (Zhang *et al.* 2014; Anbia *et al.* 2015; Chensi *et al.* 2020; Mahtab *et al.* 2020). Thiol-functionalized magnetic

doi: 10.2166/wst.2020.099

nanoparticles (MNPs) also have higher adsorption properties for Hg(II) because Hg(II) can bind strongly with sulfur-containing groups (Saman *et al.* 2014).

Ethylenediamine tetraacetic acid (EDTA) as a modification material for adsorbents has recently attracted more attention (Ren *et al.* 2013). EDTA functionalization adsorbent not only possesses good adsorption behaviors, but it also does not cause any secondary pollution. In previous studies, materials assembled with EDTA using Na_2EDTA (EDTA disodium salt) (Ren *et al.* 2013), EDTA (Liu *et al.* 2013), EDTA anhydride (Repo *et al.* 2010) and N-(trimethoxysilylpropyl)ethylenediamine triacetic acid (EDTA-silane) (Liu *et al.* 2016) have been widely investigated.

In this study, the EDTA-functionalized Fe_3O_4 (–COOH-modified magnetic materials,) was prepared using a novel method that bonded EDTA to the particle surface by polycondensation of amino and carboxyl groups, and removed Pb(II) and Cu(II) from aqueous solutions under various experimental conditions.

MATERIALS AND METHODS

Raw materials

Sodium hydroxide, ferric chloride hexahydrate ($FeCl_3{\cdot}6H_2O$), ferrous chloride tetrahydrate ($FeCl_2{\cdot}4H_2O$), hydrochloric acid, tetraethyl orthosilicate (TEOS), ammonia solution, Na_2EDTA dihydrate and metal nitrates ($Cu(NO_3)_2{\cdot}5H_2O$, $Pb(NO_3)_2$, $Cd(NO_3)_2{\cdot}4H_2O$,) were purchased from Chengdu Chron Chemicals China. 3-Aminopropyltrimethoxysilane (APTMS) was obtained from Tokyo Chemical Industry Japan. N-(3-Dimethylaminopropyl)-N′-ethylcarbodiimide hydrochloride (EDCI) and 1-hydroxybenzotriazole monohydrate (HoBt) were supplied by Aladdin Reagent, China. All the reagents were of analytical grades and used as received without further purification. All solutions were prepared using de-ionized (DI) water.

Characterization

The phase structures were analyzed using XRD (Dang Dong Fang Yuan, DX-2600, China) with Cu Kα radiation. The functional groups' infrared spectra were obtained with a TENSOR 27 Fourier transform infrared spectrometer (FTIR, Bruker Optics, TENSOR 27, Germany). The morphology and the sizes of the reluctant products were characterized using a field emission-scanning electron microscopy (FE-SEM, ZEISS, Germany). Thermogravimetric analysis (TGA) was carried out using a thermal analyzer (Mettler Toledo, TGA, Switzerland) at the heating rate of 15 °C min^{-1} under a dynamic nitrogen atmosphere flow. Hysteresis loops were recorded at room temperature with a vibrating sample magnetometer (VSM, Quantum Design, USA). An 5100 Synchronous Vertical Dual View inductively coupled plasma–optical emission spectrometer (ICP–OES, Agilent, USA) was used to test the concentrations of metal ions.

Adsorption experiments

Adsorption experiments were generally carried out by agitating the tubes containing 10.0 mL solution of heavy metal ions and 10.0 mg adsorbent on a rotary shaker. The effect of pH was conducted in metal ion concentrations of 0.5 mM at 30 °C. The pH values of the solutions were adjusted using 0.01 M hydrochloric acid and/or sodium hydroxide aqueous solutions. The metal concentration in the supernatants was analyzed using the ICP–OES after the adsorbent was removed with the help of a permanent magnet (Nd–Fe–B type, N35 grade). Adsorption capacities (q_e, mmol g^{-1}) were calculated as follows:

$$q_e = \frac{C_0 - C_e}{m} V \tag{1}$$

where C_0 and C_e (mM) are the initial and the equilibrium concentrations of the metal ions, respectively; V (L) is the volume of the solution; and m (g) represents the weight of the adsorbent.

RESULT AND DISCUSSION

Preparation of Fe_3O_4@SiO_2-EDTA

CMS was prepared using the raw materials mentioned earlier and the preparation process included three stages (shown in Figure 1). First, 60 mL iron salt solution (containing 5.44 g $FeCl_3{\cdot}6H_2O$ and 2.00 g $FeCl_2{\cdot}4H_2O$) was poured into a 250 mL three-neck round flask under nitrogen flow in ultrasonic bath. Then 100 mL sodium hydroxide solution (1 mol/L) was added drop by drop into the flask with slow mechanical agitation. The mixture was stirred for 0.5 h at 60 °C and left another 2 h under continues nitrogen flow. The black Fe_3O_4 nanoparticles were separated using external magnets and washed with dissolved oxygen-free water to a neutral pH and dried at 60 °C in a vacuum oven.

Second, 0.5 g Fe_3O_4 was suspended in a mixture (150 mL ethyl alcohol and 25 mL DI water) using

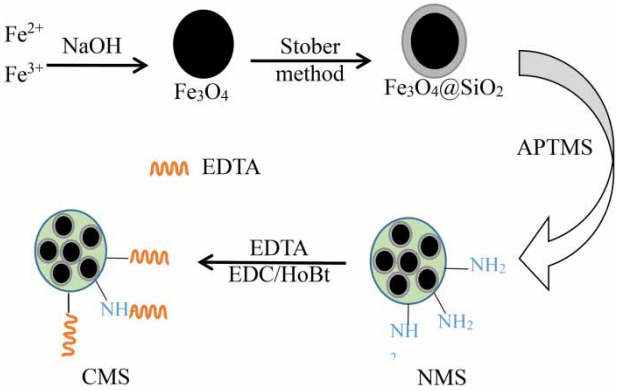

Figure 1 | The procedure for preparation of NMS and CMS.

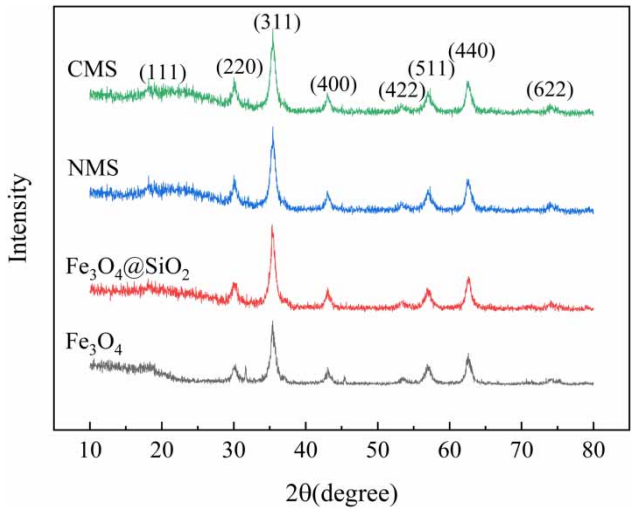

Figure 2 | XRD patterns of Fe_3O_4, SiO_2@Fe_3O_4, NMS, and CMS.

ultra-sonication for 15 min to obtain a homogeneous Fe_3O_4 dispersion. Then 3 mL of ammonia was injected whilst stirring at 30 °C. After 30 min, 2.5 mL TEOS was added and the reaction was further held under mechanical agitation for 45 min at 30 °C. After that, 0.5 ml APTMS was added and the reaction was held under mechanical agitation for 5 min at 30 °C. The black–brown nanoparticles were then rinsed with ethanol and DI water several times and $–NH_2$-modified magnetic materials (NMS) was prepared. The obtained product was separated using an external magnet, dried at 60 °C for 24 h, ground into fine powder and stored in a desiccator for further experiments.

Finally, the surface modification of NMS with EDTA was performed as follows: the as-prepared NMS (0.4 g) was dispersed in 160.0 mL DI water solution (containing 5.96 g EDTA 2Na, 1.60 g EDCI, and 0.86 g HoBt) overnight and mechanically stirred. Thus the $EDTA^{2-}$ ions were adsorbed onto the NMS via the electrostatic attraction between the protonation of amino groups of NMS and anionic moiety of carboxyl groups of EDTA; the reaction of the carboxyl groups of EDTA with the amino groups on NMS was completed using a small amount of EDCI as a cross-linker; and the addition of HoBt increased the condensation yield of the reaction. The products were rinsed with DI water several times, dried in the vacuum oven at 50 °C for 12 h, and then stored in the desiccator.

Characterization of Fe_3O_4@SiO_2-EDTA

The phase structure

Figure 2 shows the X-ray diffraction (XRD) patterns of the samples, including Fe_3O_4, Fe_3O_4@SiO_2, NMS, and CMS nanoparticles. The XRD results showed that the samples had sharp peaks, which demonstrated that the prepared adsorbents have a higher crystalline nature. The characteristic diffraction peaks that appeared in Fe_3O_4 at 18.3°, 30.1°, 35.4°, 43.1°, 53.4°, 56.9, 62.5°, and 75° could be assigned to [111], [220], [311], [400], [422], [511], and [622] planes of magnetite (JCPDS card no. 19-0629), respectively, confirming that pure Fe_3O_4 has a cubic spinel structure (Larumbe *et al.* 2012; Tan *et al.* 2014). No more peaks were assigned to the crystalline form in Fe_3O_4@SiO_2 NMS and CMS These characteristic diffraction peaks observed for the samples of Fe_3O_4@ SiO_2, NMS, and CMS indicated that Fe_3O_4 was present in Fe_3O_4@SiO_2, NMS, and CMS, and the whole preparation processes did not result in the phase change of Fe_3O_4, implying that Fe_3O_4@SiO_2, NMS, and CMS nanoparticles retained the crystalline cubic spinel structure (Kassaee *et al.* 2011).

The FTIR analysis

Figure 3 showed the FTIR spectra of Fe_3O_4, Fe_3O_4@SiO_2, NMS, and CMS nanoparticles. The typical absorption peak at 577 cm^{-1} and 1,634 cm^{-1} is attributed to the stretching vibration of Fe–O bond (Tan *et al.* 2014). For Fe_3O_4@SiO_2, the Fe–O peak decreased in Fe_3O_4@SiO_2, confirming that the functional groups successfully coated the Fe_3O_4 surface. The presence of the peak at 3,405 cm^{-1} is due to the stretching vibrations of O–H and N–H bonds (Repo *et al.* 2011). Si–O–Si bands, which were generated from oligomerization of the silanes, as well as Si–OH were also found in Fe_3O_4@SiO_2. As shown in Figure 3, the peak at 1,085 cm^{-1} was related to Si–O–C and symmetric Si–O–Si stretching

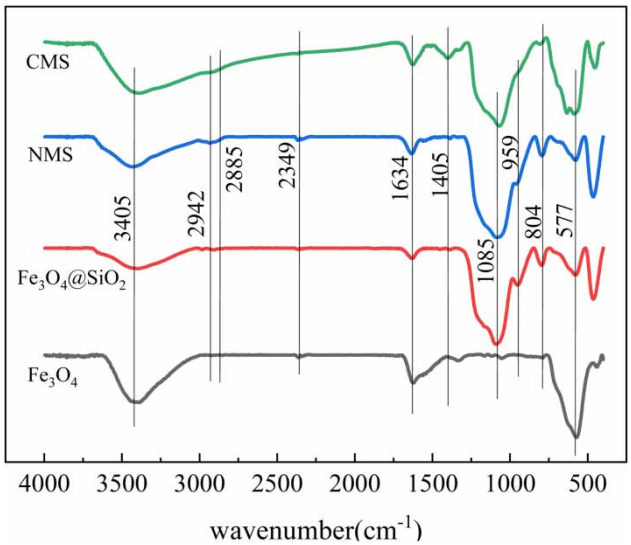

Figure 3 | FTIR spectra of Fe_3O_4, Fe_3O_4@SiO_2, NMS, and CMS.

vibrations, and the peaks at 959 cm^{-1} and 804 cm^{-1} were related to Si–OH and asymmetric Si–O–Si stretching, respectively (Repo *et al.* 2011; Dupont *et al.* 2014; Tan *et al.* 2014), implying the successful formation of silica layers on Fe_3O_4. For NMS, the presence of two new bands at 2,942 cm^{-1} and 2,885 cm^{-1} was associated with stretching of methylene groups, indicating the successful grafting of APTMS (Hou *et al.* 2010). The spectra of CMS shows a strong absorption peak at 1,405 cm^{-1} due to the stretching vibration of C=O in symmetrical –COOH groups, and this peak could be also assigned to the C–N bond and γ_{CH2} group (Hou *et al.* 2010; Huang & Keller 2015). Moreover, compared with the two spectra lines of Fe_3O_4@SiO_2 and NMS, CMS has a distinct enhanced absorption peak at 1,634 cm^{-1}, which is caused by the C=O stretching vibrations of the asymmetric COO– (Repo *et al.* 2011). All these phenomena indicate that EDTA successfully coated the surface of magnetite nanoparticles, and the carboxyl modification was completed. 2,349 cm^{-1} is an asymmetric stretching peak of CO_2 in the air.

Figure 4 presents the SEM micrographs of Fe_3O_4, Fe_3O_4@SiO_2, NMS, and CMS. All synthesized adsorbents have spherical shapes with individual particles, and there are also distinguished morphological differences. The particle size was in the following order

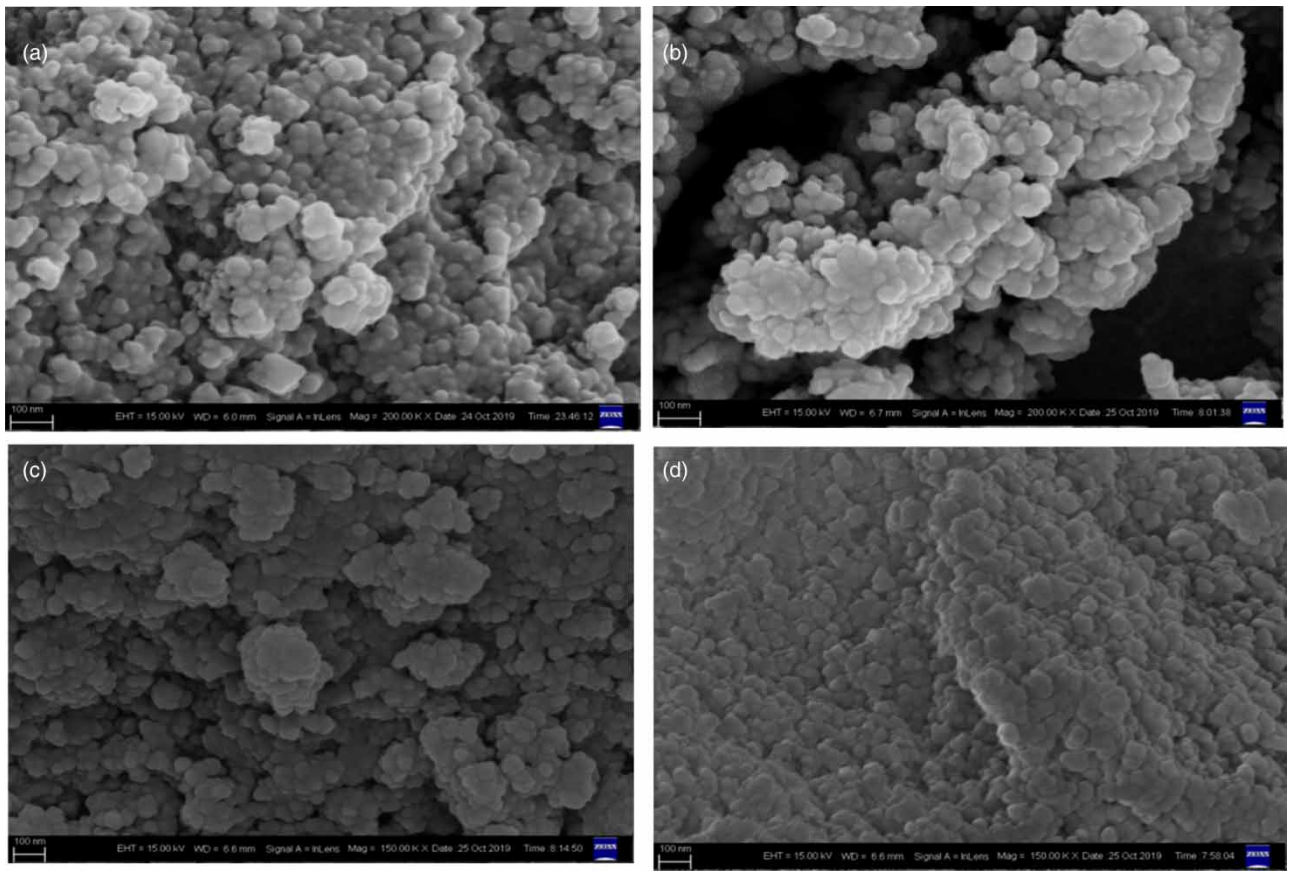

Figure 4 | SEM micrographs of (a) Fe_3O_4, (b) Fe_3O_4@SiO_2, (c) NMS, and (d) CMS.

CMS > NMS > Fe_3O_4@SiO_2 > Fe_3O_4, which was ascribed to the groups loaded onto their surfaces.

TGA analysis and magnetic measurement

For further investigation of functionalized Fe_3O_4 properties, TGA analysis of the nanoparticles was performed to determine the quantity of the grafted EDTA materials (shown in Figure 5) (Fan *et al.* 2011). It was found that the TGA curves of Fe_3O_4 and Fe_3O_4@SiO_2 nanoparticles changed slightly and the TGA curves of NMS and CMS nanoparticles changed rapidly with the temperature increase. For Fe_3O_4 nanoparticles, the weight loss was about 5.06% at temperature ranging from 30 °C to 1,000 °C, which was caused by the escape of physically adsorbed water and/or structure water on the surface (Wang *et al.* 2010). The TGA curve of Fe_3O_4@SiO_2 showed that the weight loss was about 4.90% below 200 °C due to the release of moisture on the surface of the silica layer, while the weight loss was about 2.98% at temperature ranging from 200 °C to 1,000 °C, which was related to the structure water (Wang *et al.* 2010). For the TGA curves of NMS and CMS, organic polymers on NMS and CMS began to degrade rapidly above 250 °C in addition to water loss, which is similar to the temperature at which degrading begins for cross-linked magnetic cross-linked magnetic chitosan–diacetylmonoxime Schiff's base resin (CMSO) as reported by Monier *et al.* (Fan *et al.* 2011). The organic polymers were almost completely decomposed at 1,000 °C for NMS and 950 °C for CMS, respectively. A weight loss of about 12.80 wt.% (taken off the structure water) from 200 °C to 1,000 °C in NMS, and a weight loss of about 22.52 wt.% (taken off the structure water) from 200 °C to 950 °C in CMS was used to estimate the weight proportions of cross-linked amino-groups on NMS and EDTA-modified carboxyl-group on CMS, respectively. The weight proportion of polymers on CMS (22.52 wt.%) was higher than that on NMS (12.80 wt.%). This result further verified that EDTA was modified successfully on the surface of NMS.

Figure 6 shows the magnetic hysteresis loop of Fe_3O_4, Fe_3O_4@SiO_2, NMS, and CMS nanoparticles. The saturation magnetization was 60.82, 45.52, 22.40, and 20.71 emu g^{-1}, respectively. Although the saturation magnetization values of CMS is lower than that of Fe_3O_4 and Fe_3O_4@SiO_2, CMS could be rapidly separated from their water dispersions within several seconds using the Nd–Fe–B permanent magnet (N35 grade) (seen in inset of Figure 6). These results demonstrated that CMS exhibited enough magnetic response (Fan *et al.* 2011). Moreover, the saturation magnetization decreased after functionalization, demonstrating a successful grafting of EDTA molecules onto the Fe_3O_4 surface. The weighted percentages of silica coating on Fe_3O_4, cross-linked amino-group on NMS, and EDTA-modified carboxyl-group on CMS calculated from saturation magnetization data were about 25.16%, 38.01%, and 40.79%, respectively. However, the content of EDTA on Fe_3O_4 from TGA data was not consistent with that from magnetic hysteresis loop. This could be attributed to the strong thermal stability of silicon (Liu *et al.* 2016).

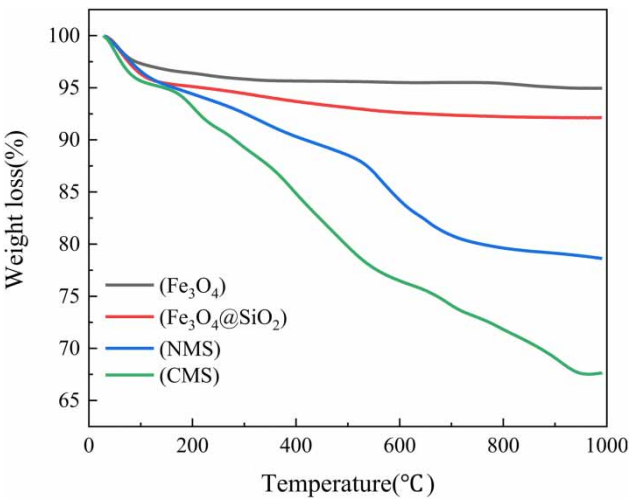

Figure 5 | TGA curves of Fe_3O_4, Fe_3O_4@SiO_2, NMS, and CMS.

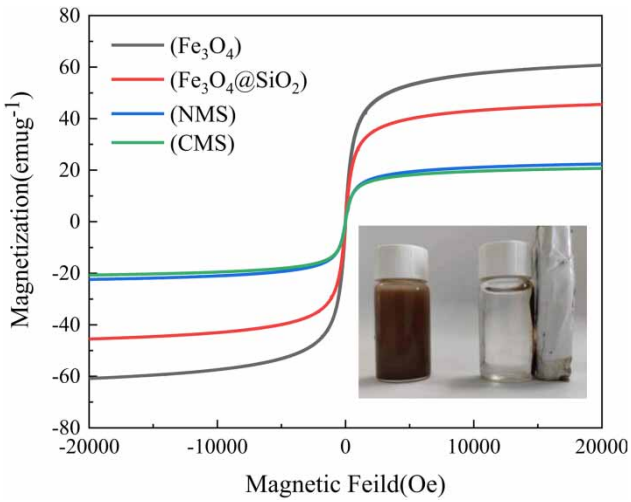

Figure 6 | Magnetic hysteresis loop of Fe_3O_4, Fe_3O_4@SiO_2, NMS, and CMS (insets: magnetic separation of CMS from the aqueous suspensions).

The adsorption properties for heavy metal

The adsorption properties of CMS for heavy metal are determined by many factors. The effect of adsorbent dosage and pH on removal of heavy metal was investigated in this work.

Effect of adsorbent dosage

The effect of dosage of CMS on the removal efficiency and adsorption capacity of Cu(II) and Pb(II) is shown in Figure 7. It was necessary to obtain the optimum adsorbent dose to maximize the interactions between metal ions and the adsorption sites of the adsorbent in the solution Hao *et al.* (2010). It can be seen that the adsorption capacities of metal ions increase with an increase of dosage of CMS. The removal efficiencies also increase greatly as the dosages of CMS increase from 0.5 g L^{-1} to 1.0 g L^{-1}, and then reach a plateau when the dosages increase from 1.0 g L^{-1} to 1.5 g^{-1}. These observations illustrate that the increase of the adsorbent dose may multiply the number of available adsorption sites, leading to the raise of the removal efficiency. However, when nearly all the heavy metals in the aqueous solutions were adsorbed by the adsorbents, the number of unoccupied active adsorption sites increased and could no longer contribute to the removal percentage, resulting in the decrease of adsorption capacities of the adsorbents (Ren *et al.* 2013). Moreover, high dosage may result in aggregation of the adsorbents (Zhou *et al.* 2009) and could further reduce the adsorption capacities of adsorbents. Therefore, as presented Figure 7, CMS exhibits better removal percentage and better adsorption capacity at the dose of 1.0 g L^{-1}, which was selected as the optimum adsorbent dose for the following experiments.

Effect of pH on Pb(II) and Cu(II) adsorption

Solution pH is an important factor affecting the interaction between sorbents and metal ions. In the water environment, pH variations can significantly affect the protonation of surface groups and speciation of metal ions. In aqueous solutions with a pH above 7, the lead (Pb) hydroxyl components are the dominant species, which would hinder the binding between metal ions and sorbents. At a pH below 7, Pb and copper (Cu) exist as Pb(II) and Cu(II), and can favorably achieve sorption onto an adsorbents' surface. In this study, experiments were performed to investigate the effect of solution pH on adsorption at a wider pH range (1–5). Figure 8 presents the effect of solution pH on Cu(II) and Pb(II) adsorption onto CMS. The adsorbent (CMS) exhibited better adsorption efficiency for Pb(II) at pH 2, but the adsorption capacities decreased with pH from 3 to pH 5. The adsorption capacity of Cu(II) followed an increasing trend from pH 2 to pH 5, as shown in Figure 8.

CONCLUSIONS

A novel magnetic adsorbent – EDTA-functionalized Fe_3O_4 (CMS) – was synthesized by polycondensation of amino and carboxyl groups and the effect on removing Pb(II) and Cu(II) from aqueous solutions was investigated.

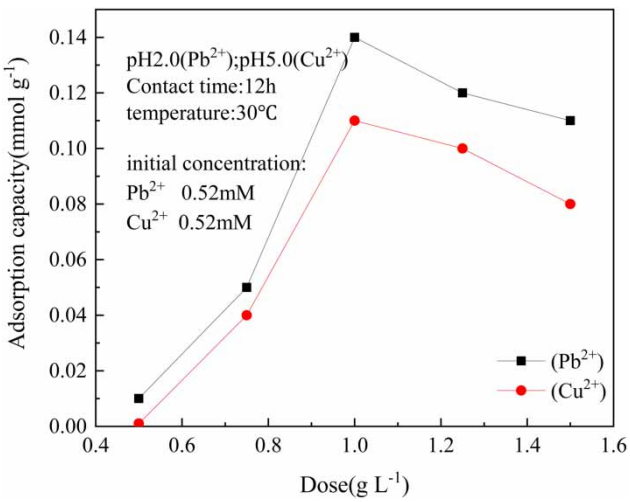

Figure 7 | Effect of adsorbent dosage on removal of heavy metal ions.

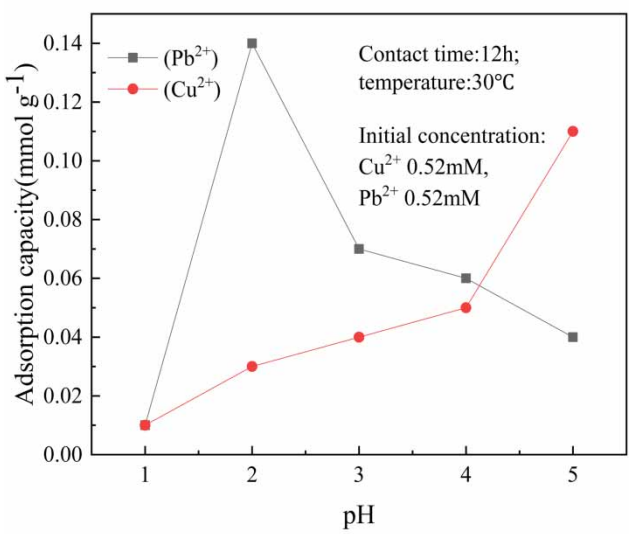

Figure 8 | Effect of pH on removal of heavy metal ions.

Characterization analyses of CMS proved EDTA successfully loaded onto Fe_3O_4. CMS showed high stability in low pH solution and good removal efficiency for heavy metal ions. The maximum adsorption capacities of CMS were 0.11 mmol g^{-1} for Cu(II) at pH5 (30 °C) and 0.14 mmol g^{-1} for Pb(II) ions at pH2 (30 °C). This study indicated that the CMS could be considered as a potential adsorbent to remove Pb(II) and Cu(II) from wastewaters at low pH.

REFERENCES

Ali, I. 2012 New generation adsorbents for water treatment. *Chemical Reviews* **112**, 5073–5091.

Anbia, M., Kargosha, K. & Khoshbooei, S. 2015 Heavy metal ions removal from aqueous media by modified magnetic mesoporous silica MCM-48. *Chemical Engineering Research and Design* **93**, 779–788.

Awual, M. R., Hasan, M. M. & Shahat, A. 2014 Functionalized novel mesoporous adsorbent for selective lead(II) ions monitoring and removal from wastewater. *Sensors and Actuators B: Chemical* **203**, 854–863.

Baccar, R., Bouzid, J., Feki, M. & Montiel, A. 2009 Preparation of activated carbon from Tunisian olive-waste cakes and its application for adsorption of heavy metal ions. *Journal of Hazardous Materials* **162**, 1522–1529.

Cegłowski, M. & Schroeder, G. 2015 Preparation of porous resin with Schiff base chelating groups for removal of heavy metal ions from aqueous solutions. *Chemical Engineering Journal* **263**, 402–411.

Cheng, Z., Gao, Z., Ma, W., Sun, Q., Wang, B. & Wang, X. 2012 Preparation of magnetic Fe_3O_4 particles modified sawdust as the adsorbent to remove strontium ions. *Chemical Engineering Journal* **209**, 451–545.

Chensi, S., Hao, L. & Yuezhong, W. 2020 Spherical Cu_2O-Fe_3O_4@chitosan bifunctional catalyst for coupled Cr-organic complex oxidation and Cr(VI) capture-reduction. *Chemical Engineering Journal* **383**, 123105.

Dong, Z., Zhang, F., Wang, D., Liu, X. & Jin, J. 2015 Polydopamine-mediated surface-functionalization of graphene oxide for heavy metal ions removal. *Journal of Solid State Chemistry* **224**, 88–93.

Dupont, D., Brullot, W., Bloemen, M., Verbiest, T. & Binnemans, K. 2014 Selective uptake of rare earths from aqueous solutions by EDTA-functionalized magnetic and nonmagnetic nanoparticles. *ACS Applied Materials & Interfaces* **6**, 4980–4988.

Fan, L., Luo, C., Lv, Z., Lu, F. & Qiu, H. 2011 Removal of Ag^+ from water environment using a novel magnetic thiourea–chitosan imprinted Ag^+. *Journal of Hazardous Materials* **194**, 193–201.

Fu, F. & Wang, Q. 2011 Removal of heavy metal ions from wastewaters: a review. *Journal of Environmental Management* **92**, 407–418.

Gode, F. & Pehlivan, E. 2006 Removal of chromium(III) from aqueous solutions using Lewatit S 100: the effect of pH, time, metal concentration and temperature. *Journal of Hazardous Materials* **136**, 330–337.

Hao, Y. M., Man, C. & Hu, Z. B. 2010 Effective removal of Cu (II) ions from aqueous solution by amino-functionalized magnetic nanoparticles. *Journal of Hazardous Materials* **184**, 392–399.

Hou, S., Su, S., Kasner, M. L., Shah, P., Patel, K. & Madarang, C. J. 2010 Formation of highly stable dispersions of silane-functionalized reduced graphene oxide. *Chemical Physics Letters* **501**, 68–74.

Huang, Y. & Keller, A. A. 2015 EDTA functionalized magnetic nanoparticle sorbents for cadmium and lead contaminated water treatment. *Water Research* **80**, 159–168.

Kassaee, M. Z., Masrouri, H. & Movahedi, F. 2011 Sulfamic acid-functionalized magnetic Fe_3O_4 nanoparticles as an efficient and reusable catalyst for one-pot synthesis of α-amino nitriles in water. *Applied Catalyst A: General* **395**, 28–33.

Kim, E. J., Lee, C. S., Chang, Y. Y. & Chang, Y. S. 2013 Hierarchically structured manganese oxide-coated magnetic nanocomposites for the efficient removal of heavy metal ions from aqueous systems. *ACS Applied Materials & Interfaces* **5**, 9628–9634.

Kong, S., Wang, Y., Hu, Q. & Olusegun, A. K. 2014 Magnetic nanoscale Fe–Mn binary oxides loaded zeolite for arsenic removal from synthetic groundwater. *Colloids and Surfaces A: Physiochemical and Engineering Aspects* **457**, 220–227.

Landaburu-Aguirre, J., Pongracz, E., Peramaki, P. & Keiski, R. L. 2010 Micellar-enhanced ultrafiltration for the removal of cadmium and zinc: use of response surface methodology to improve understanding of process performance and optimisation. *Journal of Hazardous Materials* **180**, 524–534.

Larumbe, S., Gómez-Polo, C., Pérez-Landazábal, J. I. & Pastor, J. M. 2012 Effect of a SiO_2 coating on the magnetic properties of Fe_3O_4 nanoparticles. *Journal of Physics: Condensed Matter* **24**, 266007.

Liu, Y., Chen, M. & Hao, Y. M. 2013 Study on the adsorption of Cu(II) by EDTA functionalized Fe_3O_4 magnetic nano-particles. *Chemical Engineering Journal* **218**, 46–54.

Liu, Y., Fu, R., Sun, Y., Zhou, X. X., Baig, S. A. & Xu, X. H. 2016 Multifunctional nanocomposites Fe_3O_4@SiO_2-EDTA for Pb(II) and Cu(II) removal from aqueous solutions. *Applied Surface Science* **369**, 267–276.

Mahtab, J., Asli, M. D., Taromi, F. A. & Manoochehri, M. 2020 Synthesis of multi-functionalized Fe_3O_4–NH_2–SH nanofiber based on chitosan for single and simultaneous adsorption of Pb(II) and Ni(II) from aqueous system. *International Journal of Biological Macromolecules* **148**, 201–217.

Nanseu-Njiki, C. P., Tchamango, S. R., Ngom, P. C., Darchen, A. & Ngameni, E. 2009 Mercury(II) removal from water by electrocoagulation using aluminium andiron electrodes. *Journal of Hazardous Materials* **168**, 1430–1436.

Ren, Y., Abbood H, A., He, F., Peng, H. & Huang, K. X. 2013 Magnetic EDTA-modified chitosan/SiO_2/Fe_3O_4 adsorbent: preparation, characterization, and application in heavy metal adsorption. *Chemical Engineering Journal* **226**, 300–311.

Repo, E., Warchol, J. K., Kurniawan, T. A. & Sillanpää, M. E. 2010 Adsorption of Co(II) and Ni(II) by EDTA- and/or

DTPA-modified chitosan: kinetic and equilibrium modeling. *Chemical Engineering Journal* **161**, 73–82.

Repo, E., Warchoł, J. K., Bhatnagar, A. & Sillanpää, M. 2011 Heavy metals adsorption by novel EDTA-modified chitosan-silica hybrid materials. *Journal of Colloid and Interface Science* **358**, 261–267.

Saman, N., Johari, K. & Mat, H. 2014 Synthesis and characterization of sulfur-functionalized silica materials towards developing adsorbents for mercury removal from aqueous solutions. *Microporous and Mesoporous Materials* **194**, 38–45.

Sharififard, H., Soleimani, M. & Ashtiani, F. Z. 2012 Evaluation of activated carbon and bio-polymer modified activated carbon performance for palladium and platinum removal. *Journal of the Taiwan Institute of Chemical Engineers* **43**, 696–703.

Sun, Y., Yue, Q., Gao, B., Gao, Y., Li, Q. & Wang, Y. 2013 Adsorption of hexavalent chromium on *Arundo donax Linn* activated carbon amine-crosslinked copolymer. *Chemical Engineering Journal* **217**, 240–247.

Tan, L. S., Xu, J., Xue, X. Q., Lou, Z. M., Zhu, J., Baig, S. A. & Xu, X. H. 2014 Multifunctional nanocomposites Fe_3O_4@SiO_2-mPD/SP for selective removal of Pb(II) and Cr(VI) from aqueous solutions. *RSC Advances* **4**, 45920–45929.

Wang, J., Zheng, S., Shao, Y., Liu, J., Xu, Z. & Zhu, D. 2010 Amino-functionalized Fe_3O_4@SiO_2 core–shell magnetic nanomaterial as a novel adsorbent for aqueous heavy metals removal. *Journal of Colloid and Interface Science* **349**, 293–299.

Wu, G., Kang, H., Zhang, X., Shao, H., Chu, L. & Ruan, C. 2010 A critical review on the bio-removal of hazardous heavy metals from contaminated soils: issues, progress, eco-environmental concerns and opportunities. *Journal of Hazardous Materials* **174**, 1–8.

Zargoosh, K., Zilouei, H., Mohammadi, M. R. & Abedini, H. 2014 4-Phenyl-3-thiosemicarbazide modified magnetic nanoparticles: synthesis, characterization and application for heavy metal removal. *Clean: Soil, Air, Water* **42**, 1208–1215.

Zhang, S., Zhang, Y., Bi, G., Liu, J., Wang, Z., Xu, Q. & Li, X. 2014 Mussel-inspired polydopamine biopolymer decorated with magnetic nanoparticles for multiple pollutants removal. *Journal of Hazardous Materials* **270**, 27–34.

Zhou, Y. T., Nie, H. L., Branford-White, C., He, Z. Y. & Zhu, L. M. 2009 Removal of Cu^{2+} from aqueous solution by chitosan-coated magnetic nanoparticles modified with aketoglutaric acid. *Journal of Colloid and Interface Science* **330**, 29–37.

First received 8 January 2020; accepted in revised form 22 February 2020. Available online 3 March 2020